

A comparative study of pure and copper (Cu)-doped ZnO nanorods for antibacterial and photocatalytic applications with their mechanism of action

Tamanna Bhuyan · Manika Khanuja ·
R. Sharma · S. Patel · M. R. Reddy ·
S. Anand · A. Varma

Received: 9 February 2015 / Accepted: 24 June 2015 / Published online: 7 July 2015
© Springer Science+Business Media Dordrecht 2015

Abstract The present study reports the synthesis of pure and Cu-doped ZnO nanorods for antibacterial and photocatalytic applications. The samples were synthesized by simple, low cost mechanical-assisted thermal decomposition process. The synthesized materials were characterized by scanning electron microscopy, UV–Visible spectroscopy, and photoluminescence studies. The antibacterial activity of characterized samples was determined against Gram-positive bacteria such as *Staphylococcus aureus* and *Streptococcus pyogenes* and Gram-negative bacteria such as *Escherichia coli* using shake flask method with respect to time. The significant antibacterial activity was perceived from scanning electron micrographs that clearly revealed bacterial cell lysis resulting in the release of cytoplasmic content followed by cell death. The degradation of methylene blue was used as a model organic dye for photocatalytic activity. The present study demonstrates the superior photocatalytic and

antibacterial activity of Cu-doped ZnO nanorods with respect to pure ZnO nanorods.

Keywords Doped ZnO nanorods · Antibacterial · Photocatalysis · SEM · Photoluminescence · Health effects

Introduction

In 2011, World Health Day was celebrated with the theme: “Antimicrobial resistance: No action today, No cure tomorrow”. In 2014, WHO published first global report (data provided by 114 countries) on surveillance of antimicrobial resistance (AMR) stating that antibiotics are no longer a prediction for the future (Sharma 2011). World is heading towards post-antibiotic era where infections and minor injuries which have been treatable from decades and can have lethal effect once again. Presently, AMR is a global threat because standard treatments are no longer effective, resulting in prolonged illness and greater risk of death. In order to combat increase in microbial resistance towards drug therapy, nanobioscience has gained increased attention for discovering the bactericidal effect of metal nanoparticles with various shapes and diameter (Koziej et al. 2014). This is due to the novel properties of nanomaterials including small size, large specific surface-to-volume ratio, and their close interaction and high reactivity with microbial membranes (Reddy et al. 2007).

T. Bhuyan · A. Varma
Amity Institute of Microbial Technology, Amity
University, Uttar Pradesh, Sector-125, Noida 201303,
India

M. Khanuja (✉) · R. Sharma · S. Patel ·
M. R. Reddy · S. Anand
Amity Institute of Nanotechnology, Amity University,
Uttar Pradesh, Sector-125, Noida 201303, India
e-mail: manikakhanuja@gmail.com

In recent times, zinc oxide is known for its photocatalytic driven bacterial activity. Zinc oxide is generally recognized as safe (GRAS) by food and drug administration (Rajiv et al. 2013). Till date, a great deal of research has been conducted on nano-sized ZnO particles with tremendous scientific and technological interest due to their vast list of attractive properties including biosafety, UV blocking ability, low cost, white appearance, high stability, wide direct band gap energy of 3.3 eV, and high exciton binding energy of 60 meV (Rajiv et al. 2013; Chang et al. 2012). Furthermore, many studies have reported the effective antimicrobial activity of ZnO nanoparticles against food-related bacteria (such as *Bacillus subtilis*, *Escherichia coli*, and *Pseudomonas fluorescens*), confirming their prospective applications in agricultural and food (Jiang et al. 2009). However, it has been revealed that ZnO nanostructures retain their photocatalytic activity and lose their active sites due to absence of capping agents resulting in aggregations. Moreover, the photo-oxidation rate of organic compounds present on the surface of ZnO surface is usually decreased by the high electron–hole recombination (Zhang et al. 2014). Also, at higher concentrations, Zn proves to be toxic for health besides acting as an essential element for life (Chang et al. 2012). ZnO is a wide band gap material ($E_g = 3.3$ eV) so only UV portion of sunlight can be used for generation of charge carriers. Thus, it is necessary to develop some simple and efficient procedures in order to overcome the drawbacks of the nano-sized ZnO particles, such as improving their photocatalytic efficiency along with impeding the formation of aggregations (Wang et al. 2012). Thus, ZnO usage is restricted due to its inability to use the solar spectrum effectively and high recombination rate of electron and hole. New strategies have been proposed for improving the photocatalytic efficiency of semiconductor metal oxides. These strategies include (i) tuning the band gap to use solar spectrum effectively and (ii) new range of hetrostructures and morphologies so as to reduce the recombination probability by efficient separation of photogenerated charge carriers. Many vigorous attempts have been made to synthesize nano-sized ZnO with various morphologies including rods, belts, prisms, wires, rings, flowers, and many more (Koziej et al. 2014; Zhang et al. 2014; Peng et al. 2006).

In the present work, both problems including ineffective utilization of solar spectrum and high

recombination rate of e^- and h^+ are overcome using ZnO nanorods that are doped with copper. In rod-like ZnO nanostructures, recombination probability is low due to increase in electron and hole spatial confinement. Cu doping leads to red-shift in absorption edge proving that visible part of solar spectrum also contributes to photogeneration of charge carriers (Jacob et al. 2014). Copper oxide (CuO) and zinc oxide (ZnO) NPs have been shown to exhibit tremendous potential in inhibiting the growth of a wide range of pathogenic micro-organisms (Nations et al. 2011). Additionally, till date, there are no reports revealing any bacteria developing immunity to copper as compared to the bacterial resistance developed towards many antibiotics (Theivasanthi and Alagar 2011; Santo et al. 2011). Since ages, copper nanoparticles not only attracted attention as promising antimicrobial agents, but also have been used for sterilizing textiles, liquids, and human tissues and acts as an additive in lubricants, polymers, and metallic coatings (Chatterjee et al. 2014).

Methods

Synthesis of pure ZnO and Cu-doped ZnO nanorods

Pure ZnO and Cu-doped ZnO nanorods have been prepared by mechanical-assisted thermal decomposition process (Zhang et al. 2014; Shakti et al. 2014; Noipa et al. 2014). Precursors (zinc acetate and copper acetate) were grinded (mechanical process) using a mortar–pestle for 45 min for obtaining a homogenous mixture. The mixed powder was then placed in an alumina crucible and loaded in an oven for thermal decomposition. Therefore, the synthesis process is termed as mechanical-assisted thermal decomposition process. In ZnO nanorods synthesis process, 2 g of zinc acetate dehydrate [$\text{Zn}(\text{CH}_3\text{COO})_2 \cdot 2\text{H}_2\text{O}$] was grinded using mortar–pestle for 45 min and then heated in programmable furnace (ramp rate 4 °C/min) at 500 °C for 4 h. The obtained powder sample was washed twice with distilled water and then dried in oven at 100 °C for 8 h. For preparing Cu-doped ZnO nanorods, $\text{Zn}(\text{CH}_3\text{COO})_2 \cdot 2\text{H}_2\text{O}$, and $\text{Cu}(\text{CH}_3\text{COO})_2 \cdot 2\text{H}_2\text{O}$ were used as the precursor material. The weight ratio of Cu:Zn was kept to be 10 % and then the materials were mixed in mortar–pestle until a

homogenous mixture is obtained. The resultant mixture is heated in the programmable furnace at the same 500 °C temperature for 4 h followed by the steps as mentioned above.

Characterization

The morphologies and crystallographic structure of samples were characterized by scanning electron microscopy (JEOL JSM-6010LA). The absorption spectra were measured by Perkin-Elmer UV–Visible spectrometer. The crystalline structures of ZnO and Cu-doped ZnO were investigated using X-ray diffractometer (Bruker, D2-Phaser). XRD spectrum was recorded from 5 to 80° using $\text{CuK}\alpha$ ($\lambda = 1.5403 \text{ \AA}$) X-ray operated at 10 kV and 30 mA. The Photoluminescence emission/excitation spectra were recorded at room temperature using spectrofluorometer (RF 5301 PC, SHIMAZU) with excitation wavelength of 325 nm. The emission spectra were scanned from 300 to 700 nm with a step size of 1.0 nm for both the samples.

SEM analysis of bacterial cells

Fixation of bacterial samples

Scanning electron microscopy was employed for examining the morphological changes in the bacterial cells (*Staphylococcus aureus*, *Streptococcus pyogenes*, and *E. coli*) before and after treatment with nanorod samples. Fixation of the bacterial samples was carried out with 2.5 % glutaraldehyde in 0.1 M sodium phosphate buffer, pH 7.4 for 30 min, and then incubated overnight at 4 °C. This is followed by washing the glutaraldehyde-treated samples with 0.1 M sodium phosphate buffer (pH 7.4) thrice and dehydrated with a series of 30, 50, 70, 90, and 100 % ethanol solutions. The prepared samples were then dried for 1 h at 37 °C and finally coated with a thin gold film (<10 nm). The changes in the bacterial morphology were observed under scanning electron microscope operated at a voltage of 5 kV.

Antimicrobial activity

Shake flask test in Luria Bertani (LB) broth

Preparation of bacterial cultures The antibacterial assay of the nanorod samples was determined against

both Gram-positive bacteria, *S. aureus* and *S. pyogenes*, and Gram-negative bacteria, *E. coli*. The stock bacterial cultures were maintained at 37 °C. Sterile Luria Bertani (LB) broth of 100 mL was prepared in 500-mL Erlenmeyer flasks followed by inoculation of single bacterial colonies from each of the bacterial stock cultures of *S. aureus*, *S. pyogenes*, and *E. coli*. Finally, the prepared bacterial suspensions were placed in an incubator shaker at 37 °C.

Antibacterial assay

The antibacterial activity of the nanorod samples was investigated using shake flask method. The growth inhibited by the nanoparticles was monitored as a function of time. The samples containing pure ZnO and Cu-doped ZnO nanorods (100 $\mu\text{g/mL}$) were placed in an incubator shaker at 37 °C and the variations in bacterial growth were monitored. The changes in the optical absorbance were recorded over a fixed duration of time interval (0, 3, 6, and 9 h), and the final reading was noted after 24 h of incubation at 600 nm. Antimicrobial efficacy of the bacterial species was defined as $\{[(Y - Z)/Y] \times 100\}$, where Y is the pre-inoculation bacterial count and Z is the bacterial count after treatment with the nanorod samples.

Photocatalytic studies

For photocatalysis, methylene blue (MB) was selected as a model water pollutant released by textile industry. The photocatalytic activities (degradation efficiency) of pure ZnO and Cu-doped ZnO nanorods were estimated by measuring the decomposition rate of MB. The solution was prepared by adding 5.0 mg of nanorods powder in 1000 mL of water and stirred in dark for 2 h. The samples from the solution were collected at regular intervals of time, centrifuged, and filtered. The concentration of MB was estimated in the suspension by UV–Visible spectroscopy. The absorption peak of MB is at 664 nm. The photocatalytic activity is calculated using the following relation: $\eta = \{[(C - C_0)/C_0] \times 100\}$; here, C_0 denotes the absorbance of the aqueous MB solution before the exposure, C denotes the absorbance of aqueous MB after the addition of photocatalyst and exposed for time t . The synthesized nanorods are cost-effective can be easily filtered out and are reusable after the

completion of the anticipated photocatalytic activity, hence offering the best outcomes achievable.

Results and discussion

The morphology of ZnO nanorods were investigated using scanning electron microscopy. Figure 1 shows the SEM micrograph of (a) pure ZnO nanorods and (b) Cu-doped ZnO nanorods. The zinc oxide nanorods have an average length of 500 nm and diameter 50 nm. Figure 2 shows the Tauc's plot and UV–Vis absorption spectra (inset of Fig. 2) of pure ZnO and Cu-doped ZnO nanorods. Band Gap is calculated by Tauc's relation: $\alpha = A(h\nu - E_g)^n/h\nu$, where α is the absorption coefficient, E_g is the absorption band gap, A is constant, n depends on the nature of the transitions, n may have values 1/2, 2, 3/2, and 3 corresponding to allowed direct, allowed indirect, forbidden direct, and forbidden indirect transitions, respectively. In this case, $n = 1/2$ for direct allowed transition. The band gap is obtained from the intercepts of $(\alpha h\nu)^2$ versus $(h\nu)^2$ graph. The observed band gaps are 3.35 eV for pure ZnO and 3.30 eV for doped ZnO. Observed UV spectra depicts that doping plays an important role in varying absorption characteristics of ZnO nanorods. There was a red-shift between absorption bands at 374.7 nm of pure ZnO to other absorption band at 378.2 nm of Cu-doped ZnO. The red-shift in absorption peak shows decrease in band gap of ZnO with Cu doping. Thus, red-shift in absorption edge indicates that more percentage of solar light can be utilized for electron–hole pair

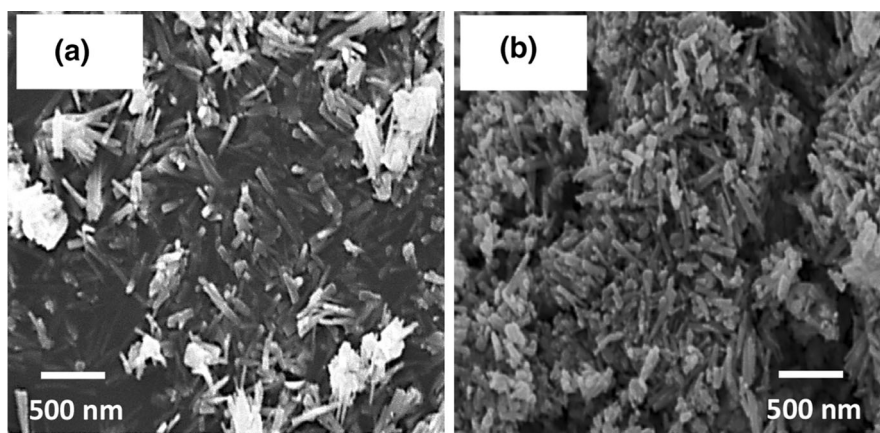


Fig. 1 SEM micrograph of **a** pure ZnO nanorods and **b** Cu-doped ZnO nanorods

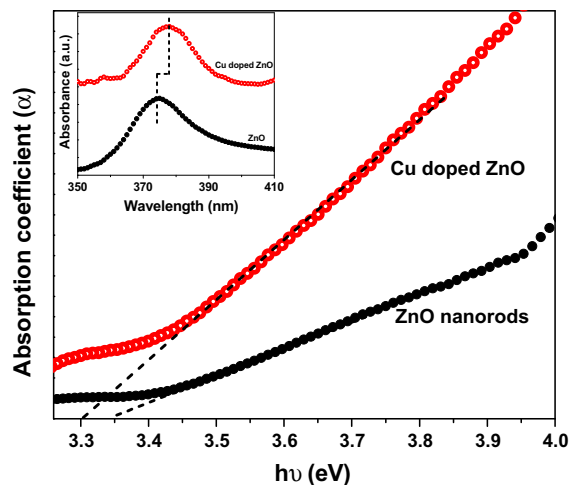


Fig. 2 Tauc plot and UV–Vis absorption spectra (inset of this figure) of pure ZnO and Cu-doped ZnO nanorods

generation (Koziej et al. 2014; Jacob et al. 2014). The band gap of ZnO nanorods was decreased from 3.35 to 3.30 eV after doping with copper. The observed red-shift in band gap (E_g) is due to Cu doping-induced band-edge bending. The change in the band gap energy is attributed to two reasons: First, the sp–d exchange interactions between sp and d orbitals of host and dopant, respectively, lead to negative correction in the conduction band and positive correction in valence band, hence overall band narrowing is observed (Ahn et al. 2007). Secondly, the electronegativity of Cu is 1.9 as compared to ZnO (which is 1.6), leading to a chemical affect in the host ZnO crystal which results in decrease in band gap.

Figure 3 shows the XRD pattern of pure ZnO and Cu-doped ZnO nanorods. All the peaks have been

labeled with (hkl) planes after comparing with JCPDS File number (06-2151). XRD pattern shows wurtzite structure with lattice constant $a = 3.247 \text{ \AA}$ and $c = 5.203 \text{ \AA}$ for ZnO and $a = 3.249 \text{ \AA}$ and $c = 5.204 \text{ \AA}$ for Cu-doped ZnO. The very slight shift in peak positions were observed with copper doping in ZnO indicating that all doped copper had gone to the substitution sites. No secondary phases viz., Cu_2O , CuO, or other metallic Cu or Zn phases were observed. Intensity of XRD peaks of Cu-doped ZnO nanorod sample was found to reduce in comparison to that of pure ZnO which indicates a decrease in crystallinity of ZnO nanorods with Cu doping.

Room-Temperature photoluminescence (PL) spectra of pure ZnO and Cu-doped ZnO nanorods sample excited at 325 nm are shown in Fig. 4a. Both pure ZnO and Cu-doped ZnO nanorods show PL characteristics in the UV and visible range. The band of PL is resolved into multiple Gaussian peaks as shown in Fig. 4b, c for ZnO and Cu-doped ZnO samples, respectively. The peaks for pure ZnO nanorod sample were observed at 399.1 nm (3.11 eV), 468.2 nm (2.65 eV), 541 nm (2.29 eV) and for Cu-doped ZnO peaks were observed at 400.5 nm (3.10 eV), 460.4 nm (2.70 eV), and 535.1 nm (2.32 eV). The slight shift in band edge peak positions in Cu-doped ZnO with respect to pure ZnO confirms the doping states in ZnO. The observed peaks at 3.11 and 3.10 eV were assigned as ultraviolet (UV) emission which is attributed to the near band-edge (NBE) free-exciton transition. The NBE emission

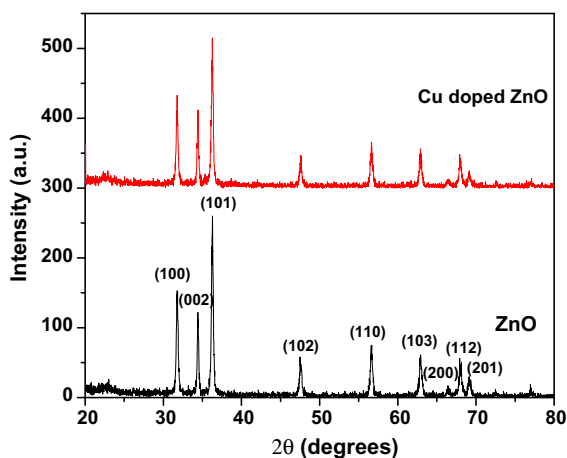


Fig. 3 XRD pattern of the two samples namely pure ZnO and Cu-doped ZnO nanorods

is a result of the exciton-associated recombination (Muthukumaran and Gopalakrishnan 2012).

The energy interval from zinc interstitial (Zn_i) to vacancy (V_{Zn}) is of the order of 2.62 eV which corresponds to blue emission at 473 nm (Xu et al. 2004). Therefore, in our samples, the prominent transition observed at 2.65 eV (468.2 nm) and 2.70 eV (460.4 nm) can be noted as the blue emission. The blue emission peak intensity increases dramatically in Cu-doped ZnO nanorods. As copper is identified to be a prominent luminescence activator, it can enhance the visible luminescence band by constructing localized states in the band gap of ZnO (Muthukumaran and Gopalakrishnan 2012; Peng et al. 2008; Lupan et al. 2011). Copper has high ionization energy and low formation energy which results in the faster incorporation of Cu into the ZnO lattice that leads to the appearance of two defective states at $E_{\text{VB}} + 0.45 \text{ eV}$ (above the valence band maximum) and $E_{\text{CB}} - 0.17 \text{ eV}$ (below the conduction band minimum). The Cu ions partially substitute the Zn ions in ZnO lattice structure and respective Zn ions enter into the interim of lattice to form interstitial defects (Zn_i). The Zn interstitial (Zn_i) and oxygen vacancy (V_o) are observed to be the dominating donor defects, whereas Zn vacancy (V_{Zn}) and oxygen interstitial (O_i) act as chief acceptor defects (Peng et al. 2008). The observed emission at 2.29 eV (541 nm) and 2.32 eV (535.1 nm) is due to the yellow emission owing to the various oxygen defects present in the sample as surface defects. These peaks can be assigned as O_i (oxygen interstitial) and V_o (oxygen vacancies). The blue and yellow emission peak intensity has increased in Cu/ZnO nanorod samples as compared to that in pure ZnO nanorods, as shown in Fig. 4c. As surface redox reactions occur on the surface of oxygen vacancies and defects, these oxygen defects are active sites of ZnO photocatalyst. These two emission peaks can enhance the electron-hole separation rate in doped ZnO nanorods.

Morphological changes in *E. coli* cells after treatment with pure ZnO and Cu-doped ZnO nanorods

SEM analysis of the prepared bacterial samples was carried out showing the changes in external morphologies of the bacterial strain. Figure 5 shows the

SEM micrograph of *E. coli* in (i) control, (ii) ZnO nanorods, (iii) Cu-doped ZnO nanorods, and (iv) magnified view of selected portion of Fig. 5iii. The untreated *E. coli* cells (control) seemed to retain their rod-shaped morphology with intact and well-

preserved cell walls and membranes as shown in Fig. 5i. In contrast, Fig. 5ii, iii shows the aggregated colonies of dead bacterial cells upon interaction with pure ZnO and Cu-doped ZnO nanorod samples. In addition, aberrant morphology of the treated cells was

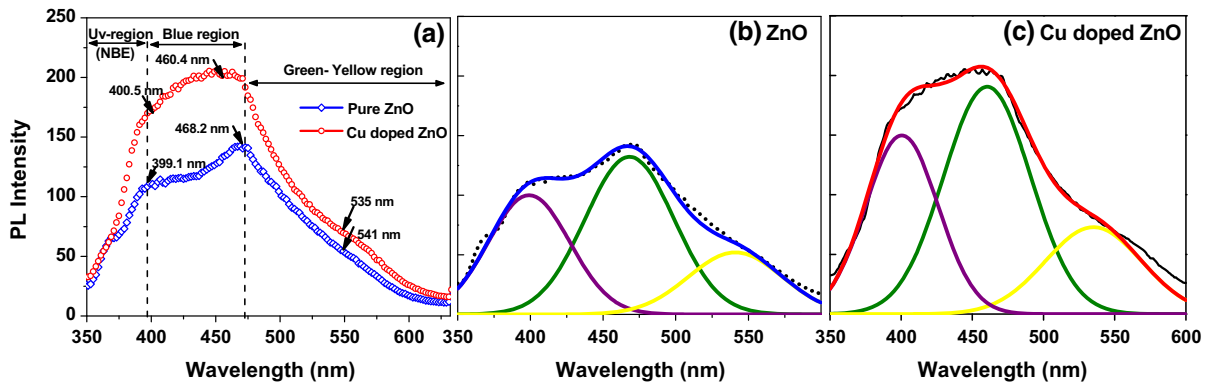


Fig. 4 a Photoluminescence (PL) spectra of pure ZnO and Cu-doped ZnO nanorods recorded at excitation wavelength 325 nm. Deconvoluted PL spectra of pure ZnO (b) and Cu-doped ZnO (c) nanorod samples

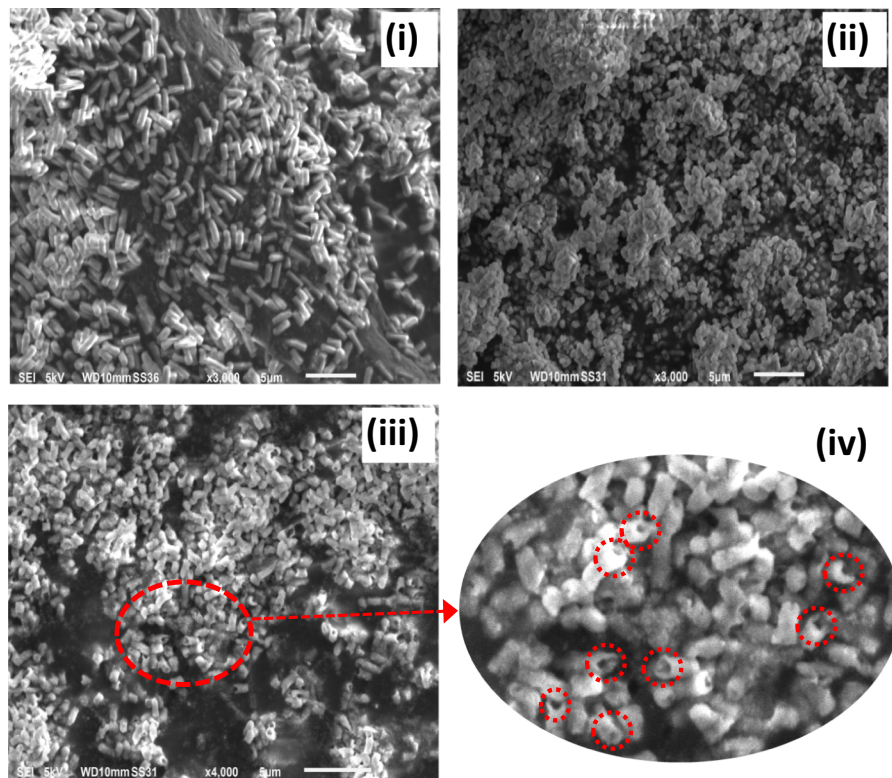


Fig. 5 SEM micrograph of *E. coli* in i control, ii ZnO nanorods, iii Cu-doped ZnO nanorods, and iv magnified view of selected portion of (iii)

accompanied by complete cellular degradation as shown. The treated *E. coli* cells undergo lysis and finally get disrupted, resulting in the release of their cytoplasmic contents into their surrounding environment. Figure 5iv clearly shows the more pronounced effect of Cu-doped ZnO nanorods on *E. coli*; clear voids had been observed in the bacterial cells that leads to loss of membrane potential.

Antibacterial activity

Comparative analysis of the antibacterial efficacy of pure ZnO and Cu-doped ZnO nanorods was carried out using shake flask method, as shown in Fig. 6 and Table 1. The antibacterial activity of pure and Cu-doped ZnO nanorods was studied as a function of time (0, 3, 6, 9 and 24 h) against Gram-positive *S. aureus* and *S. pyogenes*; as well as Gram-negative *E. coli*. Figure 6 reveals that both pure and Cu-doped ZnO samples are effective antibacterial agents on Gram-positive as well as on Gram-negative bacteria. However, percentage reduction in bacterial growth was found to be significantly higher using Cu-doped ZnO nanorods as compared to pure ZnO nanorod samples. The percentage reduction in growth was found to be $CZN_{E. coli} (61\%) > ZN_{E. coli} (37\%)$; $CZN_{S. aureus} (78\%) > ZN_{S. aureus} (70\%)$; and $CZN_{S. pyogenes} (55\%) > ZN_{S. pyogenes} (38\%)$. Interestingly,

antimicrobial action of pure and doped ZnO nanorod samples was found to be highest for *S. aureus* as compared to *E. coli* and *S. pyogenes*. Thus, the antibacterial effect of pure and doped ZnO was more pronounced for Gram-positive bacteria as compared to Gram-negative bacteria, which is in good match with the earlier studies. (Premanathan et al. 2011; Raghupathi et al. 2011; Bhuyan et al. 2015). This is explained on the basis of differences in (i) cell membrane structure, (ii) physiology and metabolic activities of the cell, and (iii) degree of contact of Gram-positive and Gram-negative bacteria (Jung et al. 2008). Additionally, Li et al. 2011 discussed the bacterial toxicity of pure and iron-doped ZnO nanoparticles in aquatic media where the Gram-negative bacteria were (*Pseudomonas putida* and *E. coli*) more resistant to the antibacterial activity of ZnO nanoparticles as compared to Gram-positive bacteria (*B. subtilis*) which holds good agreement with our results. This might be attributed due to the presence of lipopolysaccharide (LPS) layer in Gram-negative bacteria that protects the cell from a variety of toxic molecules and hence contributing to metal tolerance and sorption capacity of bacteria (Li et al. 2011).

Recent studies on Fe-doped ZnO nanoparticles have shown reduction in antimicrobial activity due to decreased shedding of Zn^{+2} as iron doping leads to stabilization of ZnO crystal structure (George et al. 2010; Fairbairn et al. 2011; Pokhrel et al. 2013). Pokhrel et al. 2013 have also reported that Fe doping adversely affects ZnO dissolution, as Fe concentration increases from 0 to 10 % and ZnO dissolution decreases from 51 to 26 %. The relatively strong σ -bonding of Fe in the host lattice of ZnO significantly reduces ZnO nanoparticle dissolution. Conversely, Cu doping is known to strain the ZnO crystal structure (Mukhtar et al. 2012), hence leading to increased dissolution of ZnO and shedding of more Zn^{+2} ions. Thus, the substitution of Cu in ZnO lattice affects the ionization of ZnO during exposure and these effects are not in line with Fe-doped ZnO.

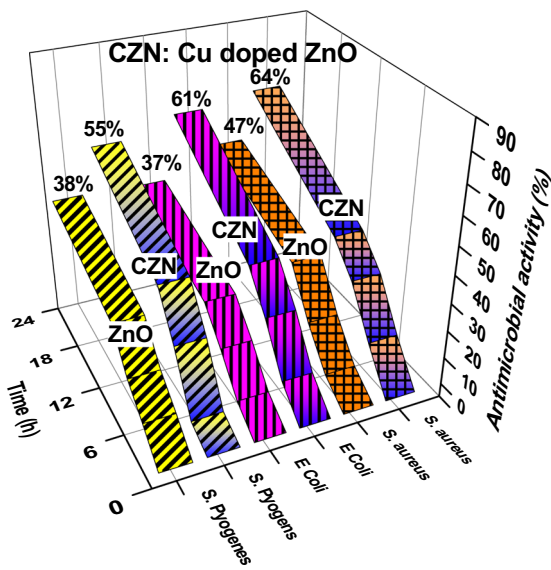


Fig. 6 Comparative analysis of the antibacterial efficacy of Pure ZnO and Cu-doped ZnO nanorods using shake flask method

Photocatalytic studies

The photocatalytic activity was performed by employing the synthesized ZnO and Cu-doped ZnO nanorods as a photocatalyst in order to study the degradation of aqueous solution of MB dye. Time-dependent UV-Vis spectra of MB dye in the presence of both ZnO and Cu-

Table 1 Antibacterial activity of pure ZnO and Cu-doped ZnO nanorods

Time (h)	Antibacterial activity (%)					
	<i>E. coli</i>		<i>S. aureus</i>		<i>S. pyogenes</i>	
	Sample ZnO	Sample CZN	Sample ZnO	Sample CZN	Sample ZnO	Sample CZN
0	0	0	0	0	0	0
3	8.3	6.1	6.2	3.7	8.5	13.4
6	15.5	16.9	17.9	22.5	23.7	28.9
9	27.2	26.4	32.8	36.6	35.5	38.2
24	37.7	36.9	46.6	54.7	60.8	64.2

CZN Cu doped ZnO nanorods

doped ZnO nanorods are shown in Fig. 7a, b, respectively. It is evident that Cu-doped ZnO nanorods lead to more efficient degradation of MB for the same exposure time as compared to pure ZnO.

Figure 7c shows the degradation efficiency (η) of both ZnO and Cu-doped ZnO nanorods as a function of time (30, 60, 90, and 120 min). The percent degradation of MB under UV irradiations using ZnO nanorods was 41.2, 58.9, 71.8, and 80.0 % at 30, 60, 90, and 120 min, respectively. Interestingly, as compared to ZnO nanorods, Cu-doped ZnO nanorods exhibited higher photocatalytic activity degrading the MB up to 97.5 % of the initial value at the end of 120 min. The percent degradation of MB using Cu-doped ZnO nanorods was recorded to be 59.1, 77.3, 88.1, and 97.5 % at 30, 60, 90, and 120 min respectively. Study of the photodegradation kinetics of MB catalyzed by pure and Cu-doped ZnO nanorods is shown in Fig. 7d. The photocatalytic activity follows the pseudo first-order kinetics and is given by

$$C_t = C_0 e^{-kt}$$

$$\text{Alternatively, } \ln \frac{C_0}{C_t} = kt$$

where C_0 is the initial concentration, C_t is the concentration after time t , and k is the rate constant of pseudo first-order reaction (Mohan et al. 2012a, b). A linear relationship between $\ln(C_0/C_t)$ and time (t) has been observed. The first-order degradation rate constants for pure ZnO and Cu-doped ZnO are found to be $k_{\text{ZnO}} = 0.0102 \text{ min}^{-1}$ and $k_{\text{Cu/ZnO}} = 0.0301 \text{ min}^{-1}$, respectively. Thus, degradation rate of MB by Cu-doped sample is three times faster as compared to pure ZnO.

The mechanism of photocatalysis for Cu-doped ZnO nanorods has been illustrated in Fig. 8. The photocatalysis process comprises three steps: Step (I) generation of electron-hole pair: The electron from the valence band gets excited to conduction band by absorbing UV light equal or higher than the band gap energy of ZnO (Eq. 1). This leads to formation of holes in valence band and electrons excited to conduction band. Copper doping results in the formation of trap levels between the valence and conduction band of ZnO. These trap levels effectively red-shift the band edge absorption threshold. In recent studies, George et al. (2011) have observed the similar enhanced absorption of near-visible light in Fe-doped TiO₂; due to trap level (vacant 3d orbitals of Fe⁺³) formations, electrons are excited to either TiO₂ conduction band or to trap levels (George et al. 2011).



Step (II) separation of electron-hole pairs and step (III) the electron- and hole-driven photo-redox reaction leads to the generation of highly active hydroxyl radical which is responsible for degradation of organic dyes (George et al. 2011; Arsana et al. 2012). The oxygen vacancy defects V_{O}^+ (Singly ionized oxygen defects), V_{O}^{++} (doubly charged state), and doped Cu nanoparticles on the surface of ZnO act as sink in improving the generated electron-hole pair separation. The released electron from the conduction band reacts with acceptors (like molecular oxygen) forming super oxide anion (Eqs. 2–5)



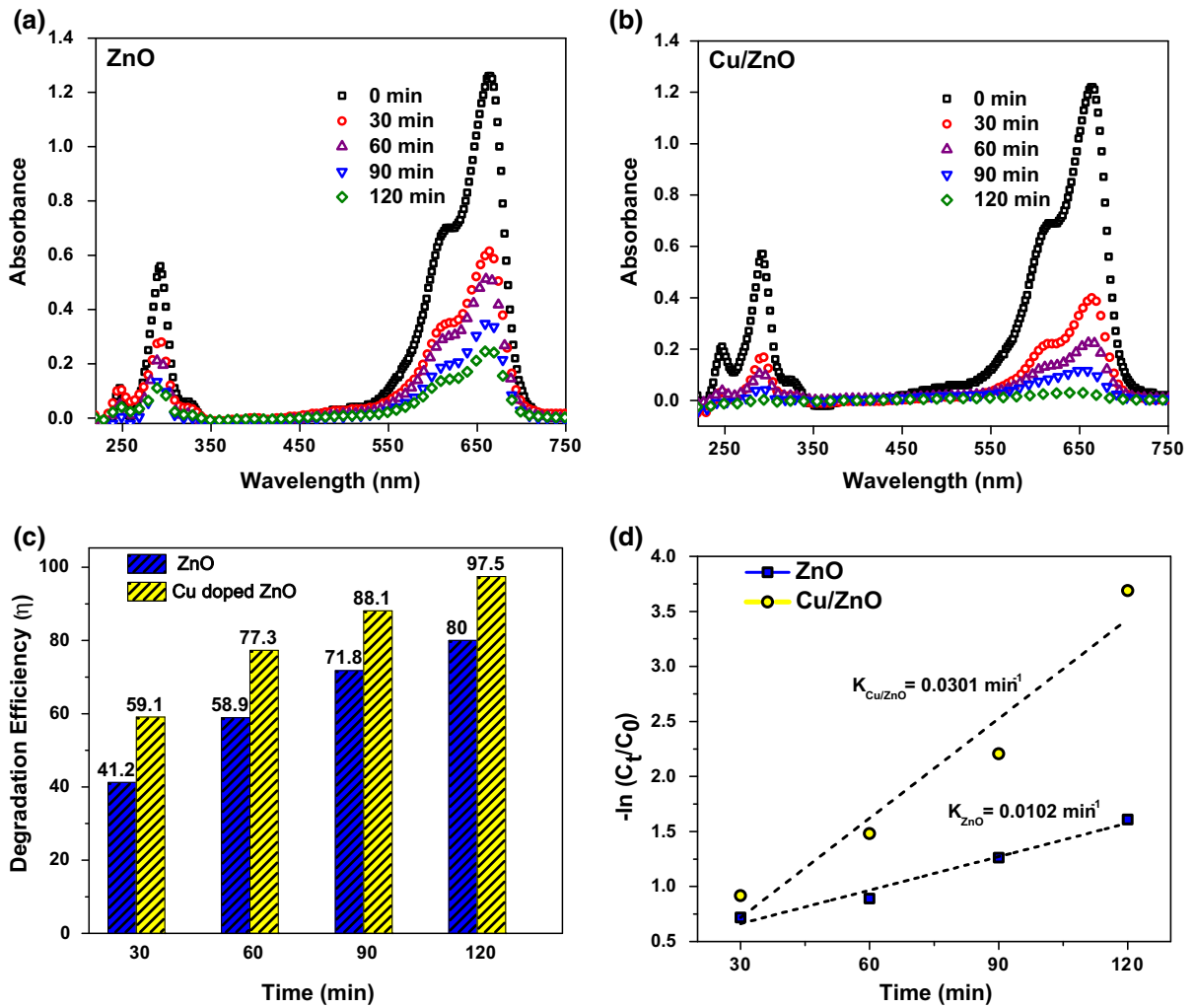
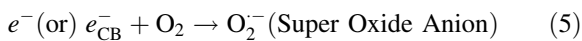


Fig. 7 a, b Time-dependent UV–Vis spectra of MB dye in the presence of pure ZnO nanorods and Cu-doped ZnO nanorods c degradation efficiency (η) as a function of time (30, 60, 90,

120 min) and corresponding d photodegradation kinetics of MB catalyzed by pure ZnO and Cu-doped ZnO nanorods



Copper ion (Cu^{+2}) takes electrons from the conduction band of ZnO decreasing the electron–hole pair recombination probability (Eq. 6), making more holes available for OH^\cdot radical formation



The holes from valence band react with (i) OH^- (moisture in air) forming OH^\cdot (hydroxyl) radical and (ii) H_2O forming OH^\cdot radical and H^+ ions (Eqs. 7, 8)



The generated $O_2^{\cdot-}$ radical reacts with H_2O forming H_2O_2 ; this further reacts with electrons from conduction band forming more OH^\cdot radicals (Eqs. 9, 10)



The formed $O_2^{\cdot-}$ and OH^\cdot undergo oxidative reaction with pollutants, i.e., organic dyes forming H_2O and CO_2 and less toxic materials (Eq. 11).

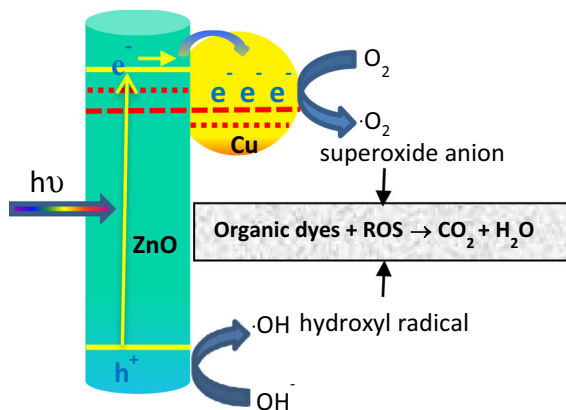
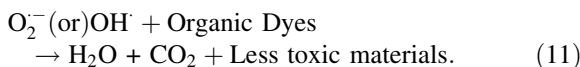


Fig. 8 The mechanism of photocatalysis for pure ZnO and Cu-doped ZnO nanorods



In consequence, enhanced photocatalytic activity in Cu-doped ZnO nanorods is attributed to (i) added rate of formation of O_2^- and OH^\cdot , and (ii) rate of electron transfer from VB of ZnO to Cu is faster than electron-hole recombination (George et al. 2011; Zhang et al. 2014; Arsana et al. 2012). Thus, Cu-doped ZnO nanorods effectively separate formed electron-hole pairs, forming more radicals and in turn enhancing the photocatalytic activity.

Conclusions

In the present work, the antibacterial and photocatalytic activity of pure and Cu-doped ZnO nanorods was investigated. Cu-doped ZnO nanorod samples showed superior antibacterial action against Gram-positive as well as Gram-negative bacteria. In addition, doped ZnO nanorods had shown better photocatalytic activity for degradation of organic water pollutants like MB. The UV-Visible results revealed that band gap undergoes a red-shift in doped ZnO nanorods as compared to pure ZnO resulting in effective utilization of solar spectrum for electron-hole pair generation. The PL results indicate that green and yellow defect emission was enhanced in doped ZnO samples leading to increase delocalization of electron hole pair.

Acknowledgments The authors are thankful to Prof. B. R. Mehta from Indian Institute of Technology Delhi, New Delhi India, Dr. R. P. Singh and Dr. Lalit M. Bharadwaj from Amity Institute of Nanotechnology (AINT), Noida (India), and Dr. V. K. Jain from Amity Institute of Advanced Research & Studies (AIARS), Amity University, Noida (India) for providing all necessary research facilities during this research work.

References

- Ahn K-S, Deutsch T, Yan Y, Jiang C-S, Perkins CL, Turner J, Jassim MAI (2007) Synthesis of band-gap-reduced p-type ZnO films by Cu incorporation. *J Appl Phys* 102:023517
- Arsana P, Bubpa C, Aroon WS (2012) Photocatalytic activity under solar irradiation of silver and copper doped zinc-oxide: photo-deposition versus liquid impregnation methods. *J Appl Sci* 12:1809–1816
- Bhuyan T, Mishra K, Khanuja M, Prasad R, Varma A (2015) Biosynthesis of zinc oxide nanoparticles from *Azadirachta indica* for antibacterial and photocatalytic applications. *Mater Sci Semicond Process* 32:55–61
- Chang YN, Zhang M, Xia L, Zhang J, Xing G (2012) The toxic effects and mechanisms of CuO and ZnO nanoparticles. *Materials* 5:2850–2871
- Chatterjee AK, Chakraborty R, Basu T (2014) Mechanism of antibacterial activity of copper nanoparticles. *Nanotechnology* 25:135101–135112
- Fairbairn EA, Keller AA, Mädler L, Zhou D, Pokhrel S, Cherra GN (2011) Metal oxide nanomaterials in seawater: Linking physicochemical characteristics with biological response in sea urchin development. *J Hazard Mater* 192:1565–1571
- George S, Pokhrel S, Xia T, Gilbert B, Ji ZX, Schowalter M, Rosenauer A, Damoiseaux R, Bradley KA, Mädler L, Nel AE (2010) Use of a rapid cytotoxicity screening approach to engineer a safer zinc oxide nanoparticle through iron doping. *ACS Nano* 4:15–29
- George S, Pokhrel S, Ji Z, Henderson BL, Xia T, Li L, Zink JI, Nel AE, Mädler L (2011) Role of Fe doping in tuning the band gap of TiO_2 for the photo-oxidation-induced cytotoxicity Paradigm. *J Am Chem Soc* 133:11270–11278
- Jacob NM, Madras G, Kottam N, Thomas T (2014) Multivalent copper doped ZnO nanoparticles with full solar spectrum absorbance and enhanced photoactivity. *Ind Eng Chem Res* 53:5895–5904
- Jiang W, Mashayekhi H, Xing B (2009) Bacterial toxicity comparison between nano- and micro-scaled oxide particles. *Environ Pollut* 157:1619–1625
- Jung WK, Koo HC, Kim KW, Shin S, Kim SH, Park YH (2008) Antibacterial activity and mechanism of action of the silver ion in *Staphylococcus aureus* and *Escherichia coli*. *Appl Environ Microbiol* 74:2171
- Koziej D, Lauria A, Niederberger M (2014) Metal oxide nanoparticles in material science. *Adv Mater* 26:235–257
- Li M, Pokhrel S, Jin X, Mädler L, Damoiseaux R, Hoek EMV (2011) Stability, bioavailability, and bacterial toxicity of ZnO and iron-doped ZnO nanoparticles in aquatic media. *Environ Sci Technol* 45:755–761
- Lupan O, Pauporté T, Viana B, Aschehoug P (2011) Electrodeposition of Cu-doped ZnO nanowire arrays and

- heterojunction formation with p-GaN for colortunable light emitting diode applications. *Electrochim Acta* 56:10543
- Mohan R, Krishnamoorthy K, Kim SJ (2012a) Diameter dependent photocatalytic activity of ZnO nanowires grown by vapor transport technique. *Chem Phys Lett* 539–540:83–88
- Mohan R, Krishnamoorthy K, Kim SJ (2012b) Enhanced photocatalytic activity of Cu-doped ZnO nanorods. *Solid State Commun* 152:375–380
- Mukhtar M, Munisa L, Saleh R (2012) Co-precipitation synthesis and characterization of nanocrystalline zinc oxide particles doped with Cu²⁺ ions. *Mater Sci Appl* 3:543–551
- Muthukumar S, Gopalakrishnan R (2012) Structural, FTIR and photoluminescence studies of Cu doped ZnO nanopowders by co-precipitation method. *Opt Mater* 34:1946–1953
- Nations S, Wages M, Cañas JE, Maul J, Theodorakis C, Cobb GP (2011) Acute effects of Fe₂O₃, TiO₂, ZnO and CuO nanomaterials on *Xenopus laevis*. *Chemosphere* 83:1053–1061
- Noipa K, Rujirawat S, Yimnirun R, Promarak V, Maensiri S (2014) Synthesis, structural, optical and magnetic properties of copper doped ZnO nanorods prepared by a simple direct thermal decomposition route. *Appl Phys A* 117:927–935
- Peng Y, Xu AW, Deng B, Antonietti M, Cölfen H (2006) Polymer-controlled crystallization of zinc oxide hexagonal nanorings and disks. *J Phys Chem B* 110:2988–2993
- Peng X, Xu J, Zang H, Wang B, Wang Z (2008) Structural and PL properties of Cu-doped ZnO films. *J Lumin* 128:297–300
- Pokhrel S, Nel AE, Mädler L (2013) Custom-designed nanomaterial libraries for testing metal oxide toxicity. *Acc Chem Res* 46:632–641
- Premanathan M, Karthikeyan K, Jeyasubramanian K, Manivannan G (2011) Selective toxicity of ZnO nanoparticles toward Gram-positive bacteria and cancer cells by apoptosis through lipid peroxidation. *Nanomedicine* 7(2):184–192
- Raghupathi KR, Koodali RT, Manna AC (2011) Size-dependent bacterial growth inhibition and mechanism of antibacterial activity of zinc oxide nanoparticles. *Langmuir* 27:4020–4028
- Rajiv P, Rajeshwari S, Venkatesh R (2013) Bio-Fabrication of zinc oxide nanoparticles using leaf extract of *Parthenium hysterophorus* L. and its size-dependent antifungal activity against plant fungal pathogens. *Spectrochim Acta A* 112:384–387
- Reddy KM, Feris K, Bell J, Wingett DG, Hanley C, Punnoose A (2007) Selective toxicity of zinc oxide nanoparticles to prokaryotic and eukaryotic systems. *Appl Phys Lett*. doi:10.1063/1.2742324
- Santo CE, Lam EW, Elowsky CG, Quaranta D, Domaille DW, Chang CJ, Grass G (2011) Bacterial killing by dry metallic copper surface. *Appl Environ Microbiol* 77:794–802
- Shakti N, Prakash A, Mandal T, Katiyar M (2014) Processing temperature dependent morphological and optical properties of ZnO nanorods. *Mater Sci Semicond Process* 20:55–60
- Sharma A (2011) Antimicrobial resistance: no action today, no cure tomorrow. *Indian J Med Microbiol* 29:91–92
- Theivasanthi T, Alagar M (2011) Studies of copper nanoparticles effects on micro-organisms. *Ann Biol Res* 2:368–373
- Wang Y, Jincheng L, Liu L, Sun DD (2012) Enhancing stability and photocatalytic activity of ZnO nanoparticles by surface modification of graphene oxide. *J Nanosci Nanotechnol* 12:1–7
- Xu CX, Sun XW, Zhang XH, Ke L, Chua SJ (2004) Photoluminescent properties of copper-doped zinc oxide nanowires. *Nanotechnology* 15:856–861
- Zhang X, Qin J, Xue Y, Yu P, Zhang B, Wang L, Liu R (2014) Effect of aspect ratio and surface defects on the photocatalytic activity of ZnO nanorods. *Sci Rep* 4:4596